

NOMA-Aided Joint Radar and Multicast-Unicast Communication Systems

Xidong Mu, *Graduate Student Member, IEEE*, Yuanwei Liu, *Senior Member, IEEE*, Li Guo, *Member, IEEE*, Jiaru Lin, *Member, IEEE*, and
Lajos Hanzo, *Fellow, IEEE*

Abstract

The novel concept of non-orthogonal multiple access (NOMA) aided joint radar and multicast-unicast communication (Rad-MU-Com) is investigated. Employing the same spectrum resource, a multi-input-multi-output (MIMO) dual-functional radar-communication (DFRC) base station detects the radar-centric users (R-user), while transmitting mixed multicast-unicast messages both to the R-user and to the communication-centric user (C-user). In particular, the multicast information is intended for both the R- and C-users, whereas the unicast information is only intended for the C-user. More explicitly, NOMA is employed to facilitate this *double spectrum sharing*, where the multicast and unicast signals are superimposed in the power domain and the superimposed communication signals are also exploited as radar probing waveforms. First, a *beamformer-based* NOMA-aided joint Rad-MU-Com framework is proposed for the system having a single R-user and a single C-user. Based on this framework, the unicast rate maximization problem is formulated by optimizing the beamformers employed, while satisfying the rate requirement of multicast and the predefined accuracy of the radar beam pattern. The resultant non-convex optimization problem is solved by a penalty-based iterative algorithm to find a high-quality near-optimal solution. Next, the system is extended to the scenario of multiple pairs of R- and C-users, where a *cluster-based* NOMA-aided joint Rad-MU-Com framework is proposed. A joint beamformer design and power allocation optimization problem is formulated for the maximization of the sum of the unicast rate at each C-user, subject to the constraints on both the minimum multicast rate for each

X. Mu, L. Guo, and J. Lin are with the Key Laboratory of Universal Wireless Communications, Ministry of Education, Beijing University of Posts and Telecommunications, Beijing 100876, China, and are also with the School of Artificial Intelligence, Beijing University of Posts and Telecommunications, Beijing 100876, China. (e-mail: muxidong@bupt.edu.cn; guoli@bupt.edu.cn; jrlin@bupt.edu.cn).

Y. Liu is with the School of Electronic Engineering and Computer Science, Queen Mary University of London, London E1 4NS, U.K. (email: yuanwei.liu@qmul.ac.uk).

L. Hanzo is with the School of Electronics and Computer Science, the University of Southampton, Southampton SO17 1BJ, U.K (e-mail: lh@ecs.soton.ac.uk).

R&C pair and on accuracy of the radar beam pattern for detecting multiple R-users. The resultant joint optimization problem is efficiently solved by another penalty-based iterative algorithm developed. Finally, our numerical results reveal that significant performance gains can be achieved by the proposed schemes over the benchmark schemes employing conventional transmission strategies.

I. INTRODUCTION

Given the rapid development of cost-efficient electronic technologies, the number of connected devices (e.g., smart phones and Internet-of-Things (IoT) nodes) in the wireless networks escalates. It is forecast that the global mobile data traffic in 2022 will be seven times of that in 2017 [1]. Moreover, new attractive applications (e.g., virtual reality (VR), augmented reality (AR), and ultra-high definition (UHD) video streaming) have emerged, which significantly improve the user-experience, but exacerbate the spectral congestion. As a remedy, a promising solution is to harness spectrum sharing between radar and communication systems [2].

Radar (which is short for “radio detection and ranging”) was originally proposed for military applications in the 1930s, and has rapidly developed in the past decades for both civilian and military applications [3]. In contrast to wireless communications, where the radio waves convey information bits, radar employs radio waves to determine the target’s characteristics (e.g., location, velocity, shape, etc.) by first transmitting probing signals and then analyzing the received echoes reflected by the target. The superior and necessity of carrying out spectrum sharing between radar and communication are summarized as follows:

- On the one hand, radar systems occupy a large amount of spectrum for both civilian and military applications [2, 4]. For instance, spectrum bands below 10 GHz, such as the S-band (2-4 GHz) and C-band (4-8 GHz), are occupied by radar systems used for weather observation. Additionally, the mmWave bands (30-300 GHz), which recently attracted extensive research interests in 5G networks, have already been used by radar systems for collision avoidance in autonomous driving and high-resolution imaging. Therefore, spectrum sharing with radar would allow communication systems to glean additional spectrum resources.
- One the other hand, the integration of radar and communication would support promising but challenging near-future applications. For instance, simultaneously supporting both radar and communication functions is essential for autonomous vehicles (AVs) [5], where the driving safety can be guaranteed via the real-time collision avoidance provided by radar and the reliable information exchange between AVs and their controllers.

A. State-of-the-art

In recent years, there have been growing research interests in communication and radar spectrum sharing (CRSS). Generally speaking, the existing research contributions may be classified into two categories: (1) radar and communication coexistence (RCC) [6] and (2) dual-function radar communication (DFRC) [7]. The key difference between the two categories is whether the radar and communication functions are facilitated by two separate systems or a common system.

1) *Studies on RCC*: The goal of RCC is to efficiently manage the mutual interference between the radar and communication systems, so that they can use the same spectrum to accomplish their own tasks. Saruthirathanaworakun *et al.* [8] proposed an opportunistic spectrum sharing scheme, where the communication system can occasionally deliver its information, when the radar spectrum is idle. Exploiting multiple antennas, Sodagari *et al.* [9] designed a multi-input-multi-output (MIMO) radar beamformer (BF) with the objective of projecting the radar probing signals into the null space of the interference channel between the radar and communication systems. Moreover, Li *et al.* [10] developed a cooperative spectrum sharing scheme for RCC, where the communication system's transmit covariance matrix and the radar sampling scheme were jointly designed for minimizing the radar's received interference power. Upon relying on realistic imperfect CSI, Liu *et al.* [11] conceived a robust BF design for RCC to improve the radar's detection performance, while satisfying the communication requirements. Qian *et al.* [12] jointly optimized the radar and communication systems for maximizing either the radar's received signal-to-interference plus noise ratio (SINR) or the communication rate achieved. In contrast to the above contributions only aiming for mitigating the interference, Liu *et al.* [13] proposed a novel symbol-level precoding scheme for RCC capable of constructively leveraging the multiuser interference. D'Andrea *et al.* [14] studied the effect of a wide-beam search based radar on the uplink performance of a massive MIMO communication system. As a further advance, Wang *et al.* [15] invoked machine learning tools for beneficially configuring the network association scheme for the communication user in RCC, where the communication throughput was maximized, while simultaneously coordinating the radar's received interference.

2) *Studies on DFRC*: As the functions of radar and communication are facilitated using a joint platform, the resultant hardware cost of DFRC is significantly reduced compared to RCC. Hence, DFRC has recently become a focal point of the CRSS research field. Hassanien *et al.* [16] exploited the sidelobe of the radar beam to embed information bits into it for communication

users. Liu *et al.* [17] proposed a pair of sophisticated strategies for implementing DFRC, namely a separated and a shared deployment, with the aim of constructing a high-quality radar beam pattern, while satisfying the communication requirements. As a further development, based on the separated and shared deployment, Dong *et al.* [18] and Liu *et al.* [19] conceived low-complexity BF design algorithms, respectively. As an innovative contribution, Liu *et al.* [20] studied the optimal waveform design of DFRC under the shared deployment paradigm, where branch-and-bound based algorithms were developed. Furthermore, Wang *et al.* [21] studied the employment of sparse arrays for DFRC, where three schemes were proposed for improving the communication performance in the presence of radar detection. Moreover, Huang *et al.* [22] and Ma *et al.* [23] employed index modulation and spatial modulation techniques for DFRC, respectively. Su *et al.* [24] studied the secure transmission for DFRC, where the radar target was treated as an eavesdropper and artificial noise was employed for degrading its received SINR, while satisfying the communication requirements of the legitimate users. To reveal the fundamental performance limits of DFRC, Chen *et al.* [25] proposed a Pareto optimization framework, where a performance region was defined relying on the difference between the peak and sidelobe (DPSL) of the radar and the SINR achieved by the communication user.

B. Motivations and Contributions

On the one hand, despite the fact that CRSS allows the communication systems to occupy more spectral resources, it is still essential to further improve the spectral efficiency (SE) for satisfying the stringent communication requirements of next-generation wireless networks. In this context, non-orthogonal multiple access (NOMA) is regarded as a promising technique of improving the communication performance, which also shares the idea of “spectrum sharing” [26, 27]. By employing superposition coding (SC) and successive interference cancellation (SIC) at the transmitters and receivers, respectively, NOMA allows multiple users to share the same frequency resources and distinguishes them in the power domain. Compared to orthogonal multiple access (OMA), NOMA can benefit CRSS by serving more users and hence achieving higher SE. On the other hand, note that the aforementioned research contributions on CRSS only considered unicast communications and assumed that the radar target does not communicate, it merely has to be detected. This paradigm represents a pair of *isolated* systems. Given the diverse future applications of wireless networks, more sophisticated CRSS schemes have to be conceived for supporting mixed multicast-unicast communication and simultaneously communicating with and

detecting the radar target user. To this end, the employment of NOMA can provide flexible resource allocation and information transmission options for CRSS. Nevertheless, to the best of our knowledge, the interplay between NOMA as well as CRSS and the potential performance gain have not been studied, which provides the main motivation of this work.

Against the above background, we propose the novel concept of NOMA-aided joint radar and

TABLE I: Our contributions in contrast to the state-of-the-art.

	[16]	[17]	[18, 19]	[20]	[24]	Proposed
Single Radar target	√	√	√, but not mentioned	√	√	√
Multiple Radar targets	×	√	√	√	×	√
Radar target communication requirement	×	×	×	×	×	√
Single communication user	√	√, but not mentioned	√			
Multiple communication users	×	√	√	√	√	√
Unicast transmission	×	√	√	√	√	√
Multicast transmission	×	×	×	×	×	√
The employment of NOMA	×	×	×	×	×	√

multicast-unicast communication (Rad-MU-Com) and investigate the corresponding radar and communication BF design problems. The main contributions of this paper can be summarized below, which are boldly and explicitly contrasted to the relevant state-of-the-art in Table I.

- We investigate a NOMA-aided joint Rad-MU-Com system, which consists of two types of users, namely the radar-centric users (R-user) and the communication-centric users (C-user). By employing power-domain NOMA, a *double spectrum sharing* operation is facilitated, where the MIMO DFRC base station (BS) transmits the mixed multicast and unicast messages to the R- and C-users, while detecting the R-user target using the transmitted superimposed communication signals.
- For the system supporting a single pair of R- and C-users, we first propose a beamformer-based NOMA (BB NOMA)-aided joint Rad-MU-Com framework, where the multicast and unicast messages are transmitted via different BFs. Based on this, we formulate a BF design problem for the maximization of the unicast rate, subject to both the multicast rate requirement and to the radar beam pattern accuracy achieved. To solve the resultant non-convex problem, we develop an efficient penalty-based iterative algorithm for finding a stationary point of the original optimization problem.
- For the system supporting multiple pairs of R- and C-users, we further propose a cluster-based NOMA (CN NOMA)-aided joint Rad-MU-Com framework, where the multicast and unicast messages for a R&C pair are superimposed at different power levels and transmitted

using a common BF. In this case, we formulate a joint BF design and power allocation problem for the maximization of the sum of the unicast rate, subject to specific constraints on the multicast rate of each R&C pair and on the radar beam pattern accuracy achieved for the detection of multiple R-user targets. The joint optimization problem formulated is efficiently solved by conceiving another developed penalty-based iterative algorithm.

- Our numerical results show that the proposed NOMA-aided joint Rad-MU-Com schemes achieve a higher unicast performance than the benchmark schemes relying on conventional transmission strategies. Furthermore, the performance gain becomes more significant, when the constraint on the radar beam pattern is more relaxed. It also shows that the proposed NOMA-aided joint Rad-MU-Com schemes are capable of supporting multicast-unicast communication, while simultaneously constructing a high-quality radar beam pattern.

C. Organization and Notation

The rest of this paper is organized as follows. In Section II, a BB NOMA-aided joint Rad-MU-Com framework is conceived for a single pair of R- and C-users. Then, a unicast rate maximization problem is formulated, which is solved by our penalty-based algorithm. In Section III, a CB NOMA-aided joint Rad-MU-Com framework is designed for multiple pairs of R- and C-users, and a unicast sum rate maximization problem is formulated and solved by the penalty-based algorithm developed. Section IV provides numerical results for characterizing the proposed schemes compared to the relevant benchmark schemes. Finally, Section V concludes the paper.

Notations: Scalars, vectors, and matrices are denoted by lower-case, bold-face lower-case, and bold-face upper-case letters, respectively; $\mathbb{C}^{N \times 1}$ denotes the space of $N \times 1$ complex-valued vectors; \mathbf{a}^H and $\|\mathbf{a}\|$ represent the conjugate transpose of vector \mathbf{a} ; $\mathcal{CN}(\mu, \sigma^2)$ denotes the distribution of a circularly symmetric complex Gaussian (CSCG) random variable with mean μ and variance σ^2 ; $\mathbf{1}$ stands for the all-one vector; $\text{Rank}(\mathbf{A})$ and $\text{Tr}(\mathbf{A})$ denote the rank and the trace of matrix \mathbf{A} , respectively; $\text{Diag}(\mathbf{A})$ represents a vector whose elements are extracted from the main diagonal elements of matrix \mathbf{A} ; $\mathbf{A} \succeq 0$ indicates that \mathbf{A} is a positive semidefinite matrix; \mathbb{H}^N denotes the set of all N -dimensional complex Hermitian matrices. $\|\mathbf{A}\|_*$, $\|\mathbf{A}\|_2$, and $\|\mathbf{A}\|_F$ are the nuclear norm, spectral norm, and Frobenius norm of matrix \mathbf{A} , respectively.

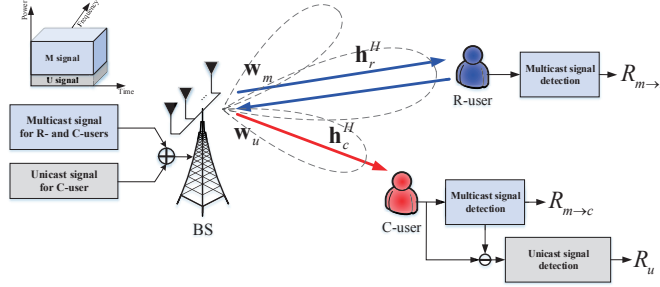


Fig. 1: Illustration of the BB NOMA-aided joint Rad-MU-Com system.

II. BB NOMA-AIDED JOINT RAD-MU-COM SYSTEM

A. System Model

As illustrated in Fig. 1, a MIMO DFRC system is considered, which consists of a single N -antenna DFRC BS, a single-antenna R-user, and a single-antenna C-user. In contrast to existing work [17–19, 24, 25], where the DFRC BS detects the R-user located within the angles of interest while only communicating with the C-user, we consider mixed multicast-unicast transmission. To be more specific, two different types of messages have to be sent by the BS, one for both the R- and C-users, namely the multicast signal, while the unicast signal is only intended for the C-user. It is worth mentioning that this mixed multicast-unicast transmission represents the evolution of DFRC from *isolation* to *integration*. For instance, the multicast signal can be employed for broadcasting group-oriented system configurations and automatic software updates, which are requested both by the R- and C-users. By contrast, the unicast signal consists of personalized voice and video traffic intended for the C-user, which is not relevant for the R-user. To support this novel concept for DFRC, we propose a BB NOMA-aided joint Rad-MU-Com framework. In the following, the communication model and radar model of the proposed system will be introduced.

1) *BB NOMA-aided MU-Communication Model*: For supporting our mixed multicast-unicast based MIMO DFRC system, the BB NOMA scheme of [28] is employed. Explicitly, the BS employs different BFs for transmitting the multicast signal intended for both R- and C-users and for the unicast signal only intended for the C-user, where the pair of signals are multiplexed in the power domain. Let $s_m[n]$ and $s_u[n]$ denote the multicast signal and the unicast signal at the time index n , respectively. Therefore, the corresponding transmitted superimposed signal at the

n th time index is given by

$$\mathbf{x}_1[n] = \mathbf{w}_m s_m[n] + \mathbf{w}_u s_u[n], \quad (1)$$

where $\mathbf{w}_m \in \mathbb{C}^{N \times 1}$ and $\mathbf{w}_u \in \mathbb{C}^{N \times 1}$ represents the BFs designed for transmitting the multicast and unicast information symbols, respectively. Without loss of generality, we assume that the multicast and unicast signals are statistically independent of each other and we have $s_m[n] \sim \mathcal{CN}(0, 1)$ and $s_u[n] \sim \mathcal{CN}(0, 1)$. Let $\mathbf{h}_r^H \in \mathbb{C}^{1 \times N}$ and $\mathbf{h}_c^H \in \mathbb{C}^{1 \times N}$ denote the BS-R-user channel and the BS-C-user channel, respectively, which are assumed to be perfectly estimated. For the R- and C-users, the signal received at time index n can be respectively expressed as

$$y_r[n] = \mathbf{h}_r^H (\mathbf{w}_m s_m[n] + \mathbf{w}_u s_u[n]) + z_r[n], \quad (2)$$

$$y_c[n] = \mathbf{h}_c^H (\mathbf{w}_m s_m[n] + \mathbf{w}_u s_u[n]) + z_c[n], \quad (3)$$

where $z_r[n] \sim \mathcal{CN}(0, \sigma_r^2)$ and $z_c[n] \sim \mathcal{CN}(0, \sigma_c^2)$ denote the additive white Gaussian noise (AWGN) of the R- and C-users at the time index n , respectively. Similar to the “strong” user in the conventional twin-user downlink NOMA transmission [26], the potentially stronger multicast signal is detected first at the C-user. Then, the remodulated multicast signal is subtracted from the composite received signal, automatically leaving the interference-free decontaminated unicast signal behind. As a result, the achievable rate for the multicast message at the C-user is given by

$$R_{m \rightarrow c} = \log_2 \left(1 + \frac{|\mathbf{h}_c^H \mathbf{w}_m|^2}{|\mathbf{h}_c^H \mathbf{w}_u|^2 + \sigma_c^2} \right). \quad (4)$$

After subtracting the remodulated multicast signal from the composite received signal by SIC, the achievable rate for the unicast signal at the C-user is given by

$$R_u = \log_2 \left(1 + \frac{|\mathbf{h}_c^H \mathbf{w}_u|^2}{\sigma_c^2} \right). \quad (5)$$

Similar to the “weak” user in the conventional twin-user downlink NOMA transmission [26], the R-user directly detects the multicast signal by treating the unicast signal as noise. Therefore,

the achievable rate for the multicast message can be expressed as

$$R_{m \rightarrow r} = \log_2 \left(1 + \frac{|\mathbf{h}_r^H \mathbf{w}_m|^2}{|\mathbf{h}_r^H \mathbf{w}_u|^2 + \sigma_r^2} \right). \quad (6)$$

The rate of the multicast signal is limited by the lower one of the pair of communication rates, which is given by

$$R_m = \min \{R_{m \rightarrow c}, R_{m \rightarrow r}\}. \quad (7)$$

2) *BB NOMA-aided Radar Detection Model*: According to [17], the above superimposed communication signals can also be exploited as radar probing waveforms, i.e., each transmitted information symbol can also be considered as a snapshot of a radar pulse. Therefore, the radar beam pattern design is equivalent to the design of the covariance matrix of the transmitted signal, $\mathbf{x}_1 [n]$, which is given by

$$\mathbf{R}_1 = \mathbb{E} [\mathbf{x}_1 [n] \mathbf{x}_1^H [n]] = \mathbf{w}_m \mathbf{w}_m^H + \mathbf{w}_u \mathbf{w}_u^H. \quad (8)$$

Then, the transmit beam pattern used for radar detection can be expressed as

$$P(\theta) = \boldsymbol{\alpha}^H(\theta) \mathbf{R}_1 \boldsymbol{\alpha}(\theta), \quad (9)$$

where $\boldsymbol{\alpha}(\theta) = [1, e^{j\frac{2\pi d}{\lambda} \sin \theta}, \dots, e^{j\frac{2\pi d}{\lambda} (N-1) \sin \theta}]^T \in \mathbb{C}^{N \times 1}$ denotes the steering vector of the transmit antenna array, θ is the detection angle, d represents the antenna spacing, and λ is the carrier wavelength.

Remark 1. The main benefits of the proposed BB NOMA-aided joint Rad-MU-Com framework can be summarized as follows. Firstly, the employment of NOMA ensures the quality of the unicast transmission (which is usually data-hungry) for the C-user, since the inter-signal interference is canceled by SIC, see (5). Secondly, despite the presence of interference, the rate-requirement of both the R- and C-users can be readily guaranteed as a benefit of the power sharing provided by NOMA, see (4) and (6). Thirdly, the different BFs used in our BB NOMA structure provide additional degrees-of-freedom (DoFs) for our radar beam pattern design, see (8). Last but not least, NOMA facilitates *double spectrum sharing* between both the multicast and unicast as well as between radar and communication systems, thus further enhancing the SE.

Remark 2. The joint Rad-MU-Com concept may also be facilitated by existing conventional

transmission schemes. For example, the multicast and unicast signals can be successively transmitted via different time slots while detecting the R-user target, namely by a time division multiple access (TDMA) based Rad-MU-Com system. Moreover, the multicast and unicast can be transmitted via conventional BFs dispensing with SIC [17–19, 24, 25] while detecting the R-user target, namely by a CBF-No-SIC based Rad-MU-Com system. These options will serve as the benchmark schemes in our performance comparisons of Section IV.

B. Problem Formulation

Before formulating the associated optimization problem, we first introduce the concept of the ideal radar beam pattern, which can be obtained by solving the following least-squares problem [17, 29]:

$$\min_{\delta, \mathbf{R}_0} \sum_{m=1}^M |\delta P^*(\theta_m) - \boldsymbol{\alpha}^H(\theta_m) \mathbf{R}_0 \boldsymbol{\alpha}(\theta_m)|^2 \quad (10a)$$

$$\text{s.t. } \text{Diag}(\mathbf{R}_0) = \frac{P_{\max} \mathbf{1}}{N}, \quad (10b)$$

$$\mathbf{R}_0 \succeq 0, \mathbf{R}_0 \in \mathbb{H}^N \quad (10c)$$

$$\delta \geq 0, \quad (10d)$$

where $\{\theta_m\}_{m=1}^M$ denotes an angular grid covering the detector's angular range in $[-\frac{\pi}{2}, \frac{\pi}{2}]$, $\boldsymbol{\alpha}(\theta_m)$ is the corresponding steering vector, $P^*(\theta_m)$ represents the desired ideal beam pattern gain at θ_m , δ is a scaling factor, P_{\max} is the maximum transmit power budget at the MIMO DFRC BS, and \mathbf{R}_0 is the waveform's covariance matrix, when only the MIMO radar is considered. Here, (10b) guarantees that the waveform transmitted by different antennas has the same average power. It can be readily verified that the ideal radar beam pattern design problem of (10) is convex, which can be efficiently solved. Let \mathbf{R}_0^* denote the optimal solution of (10), which will be used for evaluating the performance of radar detection achieved by the joint Rad-MU-Com system considered.

Given our BB NOMA-aided joint Rad-MU-Com framework and the ideal waveform's covariance matrix \mathbf{R}_0^* , we aim for maximizing the unicast rate achieved at the C-user, while satisfying the minimum rate requirement of multicast communication at both the R- and C-users as well as achieving the desired beam pattern for radar detection. The resultant optimization problem

can be formulated as follows:

$$\max_{\mathbf{w}_m, \mathbf{w}_u, \mathbf{R}_1} R_u \quad (11a)$$

$$\text{s.t. } R_m \geq \bar{R}_m, \quad (11b)$$

$$\|\mathbf{R}_1 - \mathbf{R}_0^*\|_F^2 \leq \bar{\gamma}_b, \quad (11c)$$

$$\text{Diag}(\mathbf{R}_1) = \frac{P_{\max} \mathbf{1}}{N}, \quad (11d)$$

where \bar{R}_m represents the minimum rate requirement of multicast, and $\bar{\gamma}_b$ is the maximum tolerable mismatch between the covariance matrix designed (i.e., \mathbf{R}_1) and the ideal one (i.e., \mathbf{R}_0^*).

C. Proposed Solution

The main challenge in solving problem (11) is that the objective function and the left-hand-side (LHS) is not concave with respect to the optimization variables. To address this issue, we define $\mathbf{W}_m = \mathbf{w}_m \mathbf{w}_m^H$ and $\mathbf{W}_u = \mathbf{w}_u \mathbf{w}_u^H$, which satisfy that $\mathbf{W}_m \succeq 0$, $\mathbf{W}_u \succeq 0$, $\text{Rank}(\mathbf{W}_m) = 1$, and $\text{Rank}(\mathbf{W}_u) = 1$. Then, problem (11) can be reformulated as follows

$$\max_{\mathbf{W}_m, \mathbf{W}_u, \mathbf{R}_1} \log_2 \left(1 + \frac{\text{Tr}(\mathbf{H}_c \mathbf{W}_u)}{\sigma_c^2} \right) \quad (12a)$$

$$\text{s.t. } \text{Tr}(\mathbf{H}_c \mathbf{W}_m) - \bar{\gamma}_m \text{Tr}(\mathbf{H}_c \mathbf{W}_u) - \bar{\gamma}_m \sigma_c^2 \geq 0, \quad (12b)$$

$$\text{Tr}(\mathbf{H}_r \mathbf{W}_m) - \bar{\gamma}_m \text{Tr}(\mathbf{H}_r \mathbf{W}_u) - \bar{\gamma}_m \sigma_r^2 \geq 0, \quad (12c)$$

$$\mathbf{W}_m, \mathbf{W}_u \succeq 0, \mathbf{W}_m, \mathbf{W}_u \in \mathbb{H}^N, \quad (12d)$$

$$\text{Rank}(\mathbf{W}_m) = 1, \text{Rank}(\mathbf{W}_u) = 1, \quad (12e)$$

$$(11c), (11d), \quad (12f)$$

where (12b) and (12c) are arranged from (11b). Furthermore, we defined $\mathbf{H}_c \triangleq \mathbf{h}_c \mathbf{h}_c^H$, $\mathbf{H}_r \triangleq \mathbf{h}_r \mathbf{h}_r^H$, and $\bar{\gamma}_m = 2^{R_m} - 1$. Now, the non-convexity of the reformulated problem (12) only lies in the rank-one constraint (12e). To tackle this obstacle, a popular technique is to use semidefinite relaxation (SDR) [17]. Explicitly, we firstly solve the problem by ignoring the rank-one constraint and then apply the Gaussian randomization method for constructing a rank-one solution, if the resultant solution is not of rank-one. However, considerable performance erosion may occur due to the reconstruction. On the other hand, it cannot be guaranteed that the reconstructed rank-one solution is still feasible in terms of satisfying all other constraints of the original problem

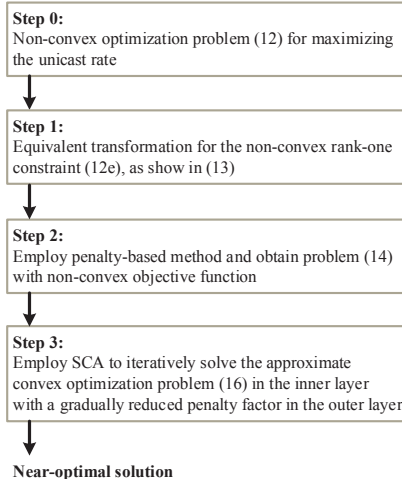


Fig. 2: Illustration of the key steps in solving problem (12).

(e.g., (11c), (12b), and (12c)). As a remedy, a double-layer penalty-based iterative algorithm is proposed for gradually finding a near-optimal rank-one solution. Before introducing the detailed manipulations, the key steps of the proposed solution for solving problem (12) are depicted in Fig. 2.

To begin with, the non-convex rank-one constraint (12e) is equivalent to the following equality constraints:

$$\|\mathbf{W}_m\|_* - \|\mathbf{W}_m\|_2 = 0, \quad (13a)$$

$$\|\mathbf{W}_u\|_* - \|\mathbf{W}_u\|_2 = 0, \quad (13b)$$

where $\|\cdot\|_*$ and $\|\cdot\|_2$ denote the nuclear norm and spectral norm of the matrix, respectively. Let us consider \mathbf{W}_m as an example. It can be verified that, for any $\mathbf{W}_m \in \mathbb{H}^N$ and $\mathbf{W}_m \succeq 0$, the above equality constraint is only satisfied, when the matrix \mathbf{W}_m is of rank-one. Otherwise, we always have $\|\mathbf{W}_m\|_* - \|\mathbf{W}_m\|_2 > 0$.

To solve problem (12), we employ the penalty-based method of [30] by introducing the transformed equality constraints for \mathbf{W}_m and \mathbf{W}_u as a penalty term into the objective function of (12), yielding the following optimization problem:

$$\min_{\mathbf{W}_m, \mathbf{W}_u, \mathbf{R}_1} -\text{Tr}(\mathbf{H}_c \mathbf{W}_u) + \frac{1}{\eta_1} \{(\|\mathbf{W}_m\|_* - \|\mathbf{W}_m\|_2) + (\|\mathbf{W}_u\|_* - \|\mathbf{W}_u\|_2)\} \quad (14a)$$

$$\text{s.t. (11c), (11d), (12b) - (12d),} \quad (14b)$$

where $\eta_1 > 0$ is the penalty factor, which penalizes the violation of the equality constraints (13a) and (13b), i.e., when \mathbf{W}_m and \mathbf{W}_u are not of rank-one. Since the maximization of R_u is equivalent to maximizing the corresponding received signal strength of $\text{Tr}(\mathbf{H}_c \mathbf{W}_u)$, we drop the log function in the objective function of (14) for simplicity. Despite relaxing the equality constraints in problem (14), it may be readily verified that the solutions obtained will always satisfy the equality constraints (i.e., have rank-one matrices), when $\frac{1}{\eta_1} \rightarrow +\infty$ ($\eta_1 \rightarrow 0$). However, if we firstly initialize η_1 with a sufficiently small value, the objective function's value of (14) tends to be dominated by the penalty term introduced, thus significantly degrading the efficiency of maximizing $\text{Tr}(\mathbf{H}_c \mathbf{W}_u)$. To facilitate efficient optimization, we can initialize η_1 with a sufficiently large value to find a good starting point, and then gradually reduce η_1 to a sufficiently small value. As a result, feasible rank-one matrix solutions associated with a near-optimal performance can eventually be obtained. In the following, we will present the details of the double-layer penalty-based algorithm for solving problem (14). In the inner layer, the optimization problem for a given η_1 is solved iteratively by employing successive convex approximation (SCA) [31] until convergence is reached. In the outer layer, the penalty factor, η_1 , is gradually reduced from a sufficiently large value to a sufficiently small one.

1) *Inner Layer: Solving Problem (14) for A Given η_1* : Note that for a given η_1 , the non-convexity of (14) manifests itself in that the second term of each penalty term is non-convex, i.e., $-\|\mathbf{W}_m\|_2$ and $-\|\mathbf{W}_u\|_2$. However, they are concave functions with respect to both \mathbf{W}_m and \mathbf{W}_u . By exploiting the first-order Taylor expansion, their upper bounds can be respectively expressed as follows:

$$-\|\mathbf{W}_m\|_2 \leq \overline{\mathbf{W}}_m^n \triangleq -\|\mathbf{W}_m^n\|_2 - \text{Tr} \left[\mathbf{v}_{\max}(\mathbf{W}_m^n) \mathbf{v}_{\max}^H(\mathbf{W}_m^n) (\mathbf{W}_m - \mathbf{W}_m^n) \right], \quad (15a)$$

$$-\|\mathbf{W}_u\|_2 \leq \overline{\mathbf{W}}_u^n \triangleq -\|\mathbf{W}_u^n\|_2 - \text{Tr} \left[\mathbf{v}_{\max}(\mathbf{W}_u^n) \mathbf{v}_{\max}^H(\mathbf{W}_u^n) (\mathbf{W}_u - \mathbf{W}_u^n) \right], \quad (15b)$$

where \mathbf{W}_m^n and \mathbf{W}_u^n denote given points during the n th iteration of the SCA method, while $\mathbf{v}_{\max}(\mathbf{W}_m^n)$ and $\mathbf{v}_{\max}(\mathbf{W}_u^n)$ represent the eigenvector corresponding to the largest eigenvalue of \mathbf{W}_m^n and \mathbf{W}_u^n , respectively.

Accordingly, by exploiting the upper bounds obtained, problem (14) can be approximated by the following convex optimization problem:

$$\min_{\mathbf{W}_m, \mathbf{W}_u, \mathbf{R}_1} -\text{Tr}(\mathbf{H}_c \mathbf{W}_u) + \frac{1}{\eta_1} \left\{ (\|\mathbf{W}_m\|_* - \overline{\mathbf{W}}_m^n) + (\|\mathbf{W}_u\|_* - \overline{\mathbf{W}}_u^n) \right\} \quad (16a)$$

$$\text{s.t. (11c), (11d), (12b) – (12d).} \quad (16b)$$

The above convex optimization problem can be efficiently solved by using existing standard convex problem solvers such as CVX [32]. Therefore, for a given η_1 , problem (16) is iteratively solved until the fractional reduction of the objective function's value in (16) falls below the predefined threshold, ϵ_i , when convergence is declared.

2) *Outer Layer: Reducing the Penalty Factor η_1* : In order to satisfy the equality constraints (13a) and (13b), in the outer layer, we gradually update the value of η_1 towards a sufficiently small value as follows:

$$\eta_1 = \varepsilon \eta_1, 0 < \varepsilon < 1, \quad (17)$$

where ε is a constant scaling factor, which has to be carefully selected for striking performance vs. complexity trade-off. For example, a larger ε allows us to explore more potential candidate solutions, thus ultimately achieving a higher final performance. This, however, in turn requires more outer iterations hence imposing a higher complexity.

3) *Overall Algorithm and Complexity Analysis*: Based on the above discussion, the proposed double-layer penalty-based procedure is summarized in **Algorithm 1**. The termination of the proposed algorithm depends on the violation of the equality constraints, which is expressed as follows:

$$\max \{ \|\mathbf{W}_m\|_* - \|\mathbf{W}_m\|_2, \|\mathbf{W}_u\|_* - \|\mathbf{W}_u\|_2 \} \leq \epsilon_o, \quad (18)$$

where ϵ_o represents the maximum tolerable value. Upon reducing η_1 , the equality constraints will finally be satisfied with the accuracy of ϵ_o . According to [31], the proposed double-layer penalty-based algorithm is guaranteed to converge to a stationary point of the original problem (11).

The main complexity of **Algorithm 1** arises from iteratively solving problem (16). Since problem (16) is a standard semidefinite program (SDP), the corresponding complexity is of the order of $\mathcal{O}(2N^{3.5})$ [33]. Therefore, the overall complexity of **Algorithm 1** is $\mathcal{O}(I_o^1 I_i^1 (2N^{3.5}))$, where I_i^1 and I_o^1 denote the number of inner and outer iterations required for the convergence of **Algorithm 1**, respectively.

Algorithm 1 Proposed double-layer penalty-based algorithm for solving problem (11)

- 1: Initialize feasible points \mathbf{W}_m^0 and \mathbf{W}_u^0 as well as the penalty factor η_1 .
 - 2: **repeat: outer layer**
 - 3: Set iteration index $n = 0$ for inner layer.
 - 4: **repeat: inner layer**
 - 5: For given \mathbf{W}_m^n and \mathbf{W}_u^n , solve the convex problem (16) and the solutions obtained are denoted by \mathbf{W}_m^* and \mathbf{W}_u^* .
 - 6: $\mathbf{W}_m^{n+1} = \mathbf{W}_m^*$, $\mathbf{W}_u^{n+1} = \mathbf{W}_u^*$, and $n = n + 1$.
 - 7: **until** the fractional reduction of the objective function value falls below a predefined threshold $\epsilon_i > 0$.
 - 8: $\mathbf{W}_m^0 = \mathbf{W}_m^*$, $\mathbf{W}_u^0 = \mathbf{W}_u^*$.
 - 9: Update $\eta_1 = \varepsilon\eta_1$.
 - 10: **until** the constraint violation falls below a maximum tolerable threshold $\epsilon_o > 0$.
-

III. CB NOMA-AIDED JOINT RAD-MU-COM SYSTEM

The joint Rad-MU-Com system of Section II serves a single pair of R- and C-users (referred to as a R&C pair), both of which require the same multicast signals¹. However, in practice, there may be multiple R&C pairs in the joint Rad-MU-Com system. In this case, the DFRC BS has to transmit multiple mixed multicast and unicast messages, while detecting multiple R-user targets. Hence, in this section we propose a CB NOMA-aided joint Rad-MU-Com framework. The key idea is to employ a common BF for conveying both the multicast and unicast messages via NOMA to the R- and C-users in one pair. Then multiple BFs are employed simultaneously for jointly detecting multiple Ruser targets in the system.

A. System Model

As shown in Fig. 3, we now consider a joint Rad-MU-Com system having $K > 1$ R&C pairs. For each pair, the DFRC BS carries out the mixed multicast and unicast transmission, i.e., transmitting a multicast message to both the R- and C-users within the same pair, while only delivering the unicast message to the C-user. Meanwhile, the DFRC BS also has to detect the K R-user targets located at different angles of interest.

1) *CB NOMA-aided MU-Communication Model*: In contrast to the BB NOMA structure of Section II, where the multicast and unicast messages are respectively transmitted via different BFs, the twinned messages are multiplexed in the power domain and they are delivered via a common BF for the intended pair [28]. Let $s_{m,k}[n]$ and $s_{u,k}[n]$ denote the multicast signal and

¹In this paper, we assume that the number of R- and C-users is the same and each R&C pair consists of a pair of R- and C-users. The problem for the system having different numbers of R- and C-users leaves as our future work.

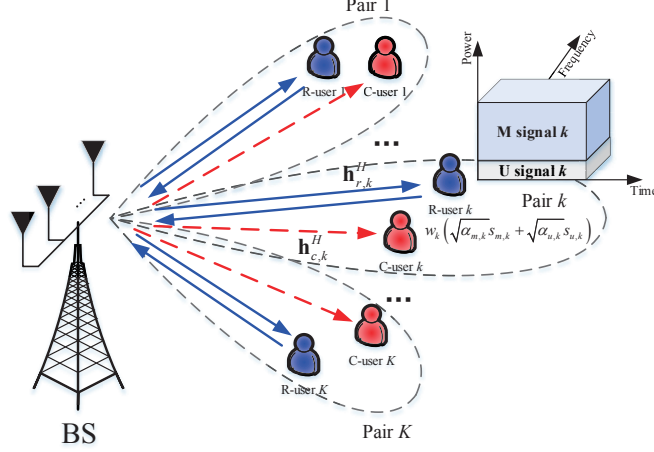


Fig. 3: Illustration of the CB NOMA-aided joint Rad-MU-Com system.

the unicast signal intended for the k th pair at the time index n , respectively, where $k \in \mathcal{K} \triangleq \{1, 2, \dots, K\}$. The BF constructed for the k th pair is denoted by $\mathbf{w}_k \in \mathbb{C}^{N \times 1}$. Therefore, the signal transmitted to the K pairs at the n th time index is given by

$$\mathbf{x}_2[n] = \sum_{k=1}^K \mathbf{w}_k \left(\sqrt{\alpha_{m,k}} s_{m,k}[n] + \sqrt{\alpha_{u,k}} s_{u,k}[n] \right), \quad (19)$$

where $\alpha_{m,k} \geq 0$ and $\alpha_{u,k} \geq 0$ denote the power allocation factor of the multicast and unicast signals of the k th pair, respectively. Without loss of generality, we have $\alpha_{m,k} + \alpha_{u,k} = 1$. Let $\mathbf{h}_{r,k}^H \in \mathbb{C}^{1 \times N}$ and $\mathbf{h}_{c,k}^H \in \mathbb{C}^{1 \times N}$ denote the channels from the BS to the R- and C-users in the k th pair, respectively, which are assumed to be perfectly estimated. Accordingly, at the time index n , the signal received by the R- and C-users in the k th pair can be respectively expressed as follows

$$\begin{aligned} y_{r,k}[n] &= \underbrace{\mathbf{h}_{r,k}^H \mathbf{w}_k \sqrt{\alpha_{m,k}} s_{m,k}[n]}_{\text{desired multicast signal}} + \underbrace{\mathbf{h}_{r,k}^H \mathbf{w}_k \sqrt{\alpha_{u,k}} s_{u,k}[n]}_{\text{intra-pair interference}} \\ &+ \underbrace{\mathbf{h}_{r,k}^H \sum_{i \neq k}^K \mathbf{w}_i \left(\sqrt{\alpha_{m,i}} s_{m,i}[n] + \sqrt{\alpha_{u,i}} s_{u,i}[n] \right) + z_{r,k}[n]}_{\text{inter-pair interference+noise}}, \quad k \in \mathcal{K}, \end{aligned} \quad (20)$$

$$\begin{aligned} y_{c,k}[n] &= \underbrace{\mathbf{h}_{c,k}^H \mathbf{w}_k \sqrt{\alpha_{m,k}} s_{m,k}[n]}_{\text{desired multicast signal}} + \underbrace{\mathbf{h}_{c,k}^H \mathbf{w}_k \sqrt{\alpha_{u,k}} s_{u,k}[n]}_{\text{desired unicast signal}} \\ &+ \underbrace{\mathbf{h}_{c,k}^H \sum_{i \neq k}^K \mathbf{w}_i \left(\sqrt{\alpha_{m,i}} s_{m,i}[n] + \sqrt{\alpha_{u,i}} s_{u,i}[n] \right) + z_{c,k}[n]}_{\text{inter-pair interference+noise}}, \quad k \in \mathcal{K}, \end{aligned} \quad (21)$$

where $z_{r,k}[n] \sim \mathcal{CN}(0, \sigma_{r,k}^2)$ and $z_{c,k}[n] \sim \mathcal{CN}(0, \sigma_{c,k}^2)$ denote the AWGN of the R- and C-users in the k th pair at the time index n , respectively.

Similarly, for each pair, downlink NOMA transmission is employed. The C-user firstly detects its intended multicast signal by treating the other signals as interference, and then detects its intended unicast signal after the SIC operation with the presence of the intra-pair interference. Therefore, the achievable rate for the intended multicast signal of the C-user in the k th pair is given by

$$R_{m \rightarrow c,k} = \log_2 \left(1 + \frac{\alpha_{m,k} |\mathbf{h}_{c,k}^H \mathbf{w}_k|^2}{\alpha_{u,k} |\mathbf{h}_{c,k}^H \mathbf{w}_k|^2 + \sum_{i \neq k}^K |\mathbf{h}_{c,k}^H \mathbf{w}_i|^2 + \sigma_{c,k}^2} \right). \quad (22)$$

After SIC, the achievable rate of the intended unicast signal at the k th C-user is given by

$$R_{u,k} = \log_2 \left(1 + \frac{\alpha_{u,k} |\mathbf{h}_{c,k}^H \mathbf{w}_k|^2}{\sum_{i \neq k}^K |\mathbf{h}_{c,k}^H \mathbf{w}_i|^2 + \sigma_{c,k}^2} \right). \quad (23)$$

Since the R-user of each pair only detects its intended multicast signal, its achievable rate in the k th pair is given by

$$R_{m \rightarrow r,k} = \log_2 \left(1 + \frac{\alpha_{m,k} |\mathbf{h}_{r,k}^H \mathbf{w}_k|^2}{\alpha_{u,k} |\mathbf{h}_{r,k}^H \mathbf{w}_k|^2 + \sum_{i \neq k}^K |\mathbf{h}_{r,k}^H \mathbf{w}_i|^2 + \sigma_{r,k}^2} \right). \quad (24)$$

Similarly, the overall multicast rate of the k th pair is given by

$$R_{m,k} = \min \{ R_{m \rightarrow c,k}, R_{m \rightarrow r,k} \}. \quad (25)$$

2) CB NOMA-aided Radar Detection Model: In this case, the covariance matrix of the transmitted signal, $\mathbf{x}_2[n]$, is given by

$$\mathbf{R}_2 = \mathbb{E} [\mathbf{x}_2[n] \mathbf{x}_2^H[n]] = \sum_{k=1}^K \mathbf{w}_k \mathbf{w}_k^H. \quad (26)$$

The transmit beam pattern constructed for radar detection can be obtained upon replacing \mathbf{R}_1 of (9) by \mathbf{R}_2 .

Remark 3. Note that the BB NOMA-aided joint Rad-MU-Com framework can also be employed for systems having $K > 1$ R&C pairs. To facilitate this design, each pair requires 2 BFs for respectively delivering the multicast and unicast messages, thus leading to a total of $2K$ BFs for our joint Rad-MU-Com system. Despite providing enhanced DoFs for system design, the

resultant complexity may become excessive, when K is large. By contrast, our CB NOMA-aided joint Rad-MU-Com framework only requires a total of K BFs for achieving the same goal at a reduced complexity, which motivates us to exploit this design.

B. Problem Formulation

In this context, aim is to maximize the sum of the unicast rate of all C-users, subject to the constraints on both the rate requirements of the multicast in each pair and on the mismatch between the achieved and the actual true beam pattern of the K R-user targets. Therefore, the optimization problem can be formulated as follows:

$$\max_{\{\mathbf{w}_k, \alpha_{m,k}, \alpha_{u,k}\}, \mathbf{R}_2} \sum_{k=1}^K R_{u,k} \quad (27a)$$

$$\text{s.t. } R_{m,k} \geq \bar{R}_{m,k}, \forall k \in \mathcal{K}, \quad (27b)$$

$$\|\mathbf{R}_2 - \mathbf{R}_0^*\|_F^2 \leq \bar{\gamma}_b, \quad (27c)$$

$$\text{Diag}(\mathbf{R}_2) = \frac{P_{\max} \mathbf{1}}{N}, \quad (27d)$$

$$\alpha_{m,k} + \alpha_{u,k} = 1, \forall k \in \mathcal{K}, \quad (27e)$$

$$\alpha_{m,k} \geq 0, \alpha_{u,k} \geq 0, \forall k \in \mathcal{K}, \quad (27f)$$

where $\bar{R}_{m,k}$ denotes the minimum required multicast rate of the k th pair and \mathbf{R}_0^* represents the actual true radar beam pattern, which can be obtained by solving problem (10) for detecting K R-users. Problem (27) is a non-convex optimization problem due to the non-convex objective function and the non-convex multicast rate constraint (27b), where the power allocation factors, $\{\alpha_{m,k}, \alpha_{u,k}\}$, and the transmit BFs, $\{\mathbf{w}_k\}$, are highly coupled. Note that for such a challenging optimization problem, it is non-trivial to find the globally optimal solution. In the following, we still invoke the penalty-based method and the SCA method to find a high-quality near-optimal solution.

C. Proposed Solution

Let us define $\mathbf{W}_k = \mathbf{w}_k \mathbf{w}_k^H$, which satisfy that $\mathbf{W}_k \succeq 0$ and $\text{Rank}(\mathbf{W}_k) = 1, \forall k \in \mathcal{K}$. Problem (27) can be reformulated as follows:

$$\max_{\{\mathbf{W}_k, \alpha_{m,k}, \alpha_{u,k}\}, \mathbf{R}_2} \sum_{k=1}^K \log_2 \left(1 + \frac{\alpha_{u,k} \text{Tr}(\mathbf{H}_{c,k} \mathbf{W}_k)}{\sum_{i \neq k}^K \text{Tr}(\mathbf{H}_{c,k} \mathbf{W}_i) + \sigma_{c,k}^2} \right) \quad (28a)$$

$$\text{s.t. } \alpha_{m,k} - \bar{\gamma}_{m,k} \alpha_{u,k} - \bar{\gamma}_{m,k} \frac{\sum_{i \neq k}^K \text{Tr}(\mathbf{H}_{l,k} \mathbf{W}_i) + \sigma_{l,k}^2}{\text{Tr}(\mathbf{H}_{l,k} \mathbf{W}_k)} \geq 0, \forall l \in \{r, c\}, k \in \mathcal{K}, \quad (28b)$$

$$\mathbf{W}_k \succeq 0, \mathbf{W}_k \in \mathbb{H}^N, \forall k \in \mathcal{K}, \quad (28c)$$

$$\text{Rank}(\mathbf{W}_k) = 1, \forall k \in \mathcal{K}, \quad (28d)$$

$$(27c) - (27f), \quad (28e)$$

where (28b) follows from (27b) with $\mathbf{H}_{l,k} \triangleq \mathbf{h}_{l,k} \mathbf{h}_{l,k}^H, \forall l \in \{r, c\}, k \in \mathcal{K}$, and $\bar{\gamma}_{m,k} = 2^{\bar{R}_{m,k}} - 1, \forall k \in \mathcal{K}$. The reformulated problem (28) is a non-convex optimization problem due to the non-convex objective function and the non-convex constraints (28b) and (28d). Similarly, the key steps of the proposed solution for solving problem (28) are depicted in Fig. 4. In the following, we first deal with the non-convex objective function and the constraint (28b).

We first introduce some auxiliary variables such that

$$\varpi_{c,k} = \frac{\alpha_{u,k} \text{Tr}(\mathbf{H}_{c,k} \mathbf{W}_k)}{\sum_{i \neq k}^K \text{Tr}(\mathbf{H}_{c,k} \mathbf{W}_i) + \sigma_{c,k}^2}, \forall k \in \mathcal{K}, \quad (29)$$

$$A_{l,k}^2 = \sum_{i \neq k}^K \text{Tr}(\mathbf{H}_{l,k} \mathbf{W}_i) + \sigma_{l,k}^2, \forall l \in \{r, c\}, \forall k \in \mathcal{K}. \quad (30)$$

Then, problem (28) can be equivalently rewritten as the following optimization problem:

$$\max_{\{\mathbf{W}_k, \alpha_{m,k}, \alpha_{u,k}, \varpi_{c,k}, A_{c,k}, A_{r,k}\}, \mathbf{R}_2} \sum_{k=1}^K \log_2(1 + \varpi_{c,k}) \quad (31a)$$

$$\text{s.t. } \alpha_{m,k} - \bar{\gamma}_{m,k} \alpha_{u,k} - \bar{\gamma}_{m,k} \frac{A_{l,k}^2}{\text{Tr}(\mathbf{H}_{l,k} \mathbf{W}_k)} \geq 0, \forall l \in \{r, c\}, k \in \mathcal{K}, \quad (31b)$$

$$\varpi_{c,k} \leq \frac{\alpha_{u,k} \text{Tr}(\mathbf{H}_{c,k} \mathbf{W}_k)}{\sum_{i \neq k}^K \text{Tr}(\mathbf{H}_{c,k} \mathbf{W}_i) + \sigma_{c,k}^2}, \forall k \in \mathcal{K}, \quad (31c)$$

$$A_{l,k}^2 \geq \sum_{i \neq k}^K \text{Tr}(\mathbf{H}_{l,k} \mathbf{W}_i) + \sigma_{l,k}^2, \forall l \in \{r, c\}, k \in \mathcal{K}, \quad (31d)$$

$$(27c) - (27f), (28c), (28d). \quad (31e)$$

This is because at the optimal solution of (31), it may be readily verified that constraints (31c) and (31d) will always be satisfied with equality. To demonstrate this, let us assume that at the optimal solution of (31), we can always increase $\varpi_{c,k}$ for ensuring that (31c) is met with strict equality if the constraint (31c) is satisfied with strict inequality. This also increases the value of the objective function. Moreover, if the constraint (31d) is satisfied with strict inequality, we can

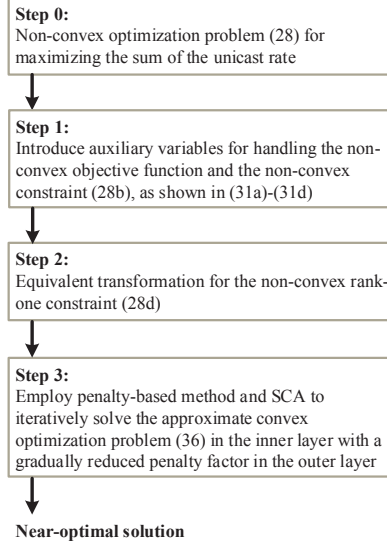


Fig. 4: Illustration of the key steps in solving problem (28).

decrease $A_{l,k}$ for ensuring that (31d) is satisfied with strict equality, without decreasing the value of the objective function at the same time. Therefore, problem (31) is equivalent to problem (28).

For problem (31), the objective function is concave with respect to $\varpi_{c,k}$ and the third term in the LHS of (31b) is concave jointly with respect to $A_{l,k}$ and $\text{Tr}(\mathbf{H}_{l,k}\mathbf{W}_k)$. However, the constraints (31c) and (31d) are non-convex with respect to the corresponding optimization variables. To handle the non-convex constraint (31c), we introduce another auxiliary variable so that

$$\varpi_{c,k} \left(\sum_{i \neq k}^K \text{Tr}(\mathbf{H}_{c,k}\mathbf{W}_i) + \sigma_{c,k}^2 \right) \leq B_{c,k}^2 \leq \alpha_{u,k} \text{Tr}(\mathbf{H}_{c,k}\mathbf{W}_k), \forall k \in \mathcal{K}. \quad (32)$$

Then, (31c) can be equivalently transformed into the following two constraints:

$$\sum_{i \neq k}^K \text{Tr}(\mathbf{H}_{c,k}\mathbf{W}_i) + \sigma_{c,k}^2 \leq \frac{B_{c,k}^2}{\varpi_{c,k}}, \forall k \in \mathcal{K}, \quad (33a)$$

$$\frac{B_{c,k}^2}{\alpha_{u,k}} \leq \text{Tr}(\mathbf{H}_{c,k}\mathbf{W}_k), \forall k \in \mathcal{K}. \quad (33b)$$

It can be observed that the constraint (33a) is non-convex, since the right-hand-side (RHS) is not concave, while the constraint (33b) is convex. However, the RHS of (33a) is a convex function joint with respect to $B_{c,k}$ and $\varpi_{c,k}$. For any given feasible points, $\{B_{c,k}^n, \varpi_{c,k}^n\}$, a lower bound

of the RHS of (33a) is given by

$$\begin{aligned} \frac{B_{c,k}^2}{\varpi_{c,k}} &\geq \frac{B_{c,k}^{n2}}{\varpi_{c,k}^n} + \frac{2B_{c,k}^n}{\varpi_{c,k}^n} (B_{c,k} - B_{c,k}^n) - \frac{B_{c,k}^{n2}}{\varpi_{c,k}^{n2}} (\varpi_{c,k} - \varpi_{c,k}^n) \\ &= \frac{2B_{c,k}^n}{\varpi_{c,k}^n} B_{c,k} - \frac{B_{c,k}^{n2}}{\varpi_{c,k}^{n2}} \varpi_{c,k} \triangleq \Gamma(B_{c,k}, \varpi_{c,k}), \forall k \in \mathcal{K} \end{aligned} \quad (34)$$

at the n th iteration of SCA by exploiting the first-order Taylor expression. For the non-convex constraint (31d), a lower bound using the first-order Taylor expression can be obtained as follows:

$$A_{l,k}^2 \geq A_{l,k}^{n2} + 2A_{l,k}^n (A_{l,k} - A_{l,k}^n) \triangleq \Upsilon(A_{l,k}), \forall l \in \{r, c\}, k \in \mathcal{K}, \quad (35)$$

since its LHS is a convex function with respect to $A_{l,k}$, where $A_{l,k}^n$ is the given feasible point at the n th iteration of the SCA.

As for the remaining non-convex rank-one constraint (28d), it can be handled in a same manner as introduced in the previous section. Therefore, by exploiting the penalty-based method as well as the above lower bounds of (34) and (35), we have the following optimization problem at the n th iteration of the SCA:

$$\min_{\mathcal{X}, \mathbf{R}_2} - \sum_{k=1}^K \log_2(1 + \varpi_{c,k}) + \frac{1}{\eta_2} \left(\sum_{k=1}^K \|\mathbf{W}_k\|_* - \overline{\mathbf{W}}_k^n \right) \quad (36a)$$

$$\text{s.t.} \quad \sum_{i \neq k}^K \text{Tr}(\mathbf{H}_{c,k} \mathbf{W}_i) + \sigma_{c,k}^2 \leq \Gamma(B_{c,k}, \varpi_{c,k}), \forall k \in \mathcal{K}, \quad (36b)$$

$$\Upsilon(A_{l,k}) \geq \sum_{i \neq k}^K \text{Tr}(\mathbf{H}_{l,k} \mathbf{W}_i) + \sigma_{l,k}^2, \forall l \in \{r, c\}, k \in \mathcal{K}, \quad (36c)$$

$$(27c) - (27f), (28c), (31b), (33b), \quad (36d)$$

where $\overline{\mathbf{W}}_k^n \triangleq -\|\mathbf{W}_k^n\|_2 - \text{Tr}[\mathbf{v}_{\max}(\mathbf{W}_k^n) \mathbf{v}_{\max}^H(\mathbf{W}_k^n) (\mathbf{W}_k - \mathbf{W}_k^n)]$, $\forall k \in \mathcal{K}$ and $\mathcal{X} \triangleq \{\mathbf{W}_k, \alpha_{m,k}, \alpha_{u,k}, \varpi_{c,k}, A_{c,k}, A_{r,k}, B_{c,k}\}$. Now, for any given penalty factor, $\eta_2 > 0$, it may be readily shown that problem (36) is a convex optimization problem, which can be efficiently solved using CVX [32]. In order to obtain feasible rank-one matrix solutions of high performance, we still develop a double-layer penalty-based algorithm. In the inner layer, problem (36) is iteratively solved by employing SCA for a given η_2 . In the outer layer, the value of η_2 is gradually decreased for ensuring that the matrix solutions obtained become of rank-one. Similarly, the algorithm terminates, when the equality constraints are satisfied with the predefined accuracy, yielding the

Algorithm 2 Proposed double-layer penalty-based algorithm for solving the joint BF design and power allocation problem (27)

- 1: Initialize feasible points $\{\mathbf{W}_k^0, \alpha_{m,k}^0, \alpha_{u,k}^0\}$ and the penalty factor η_2 .
 - 2: **repeat: outer layer**
 - 3: Set iteration index $n = 0$ for inner layer.
 - 4: **repeat: inner layer**
 - 5: Calculate the current value of $\{\varpi_{c,k}^n, A_{c,k}^n, A_{r,k}^n, B_{c,k}^n\}$ using (29), (30), and (32).
 - 6: For given feasible points, solve the convex problem (36) and the solutions obtained are denoted by $\{\mathbf{W}_k^*, \alpha_{m,k}^*, \alpha_{u,k}^*\}$.
 - 7: Update $\{\mathbf{W}_k^{n+1}, \alpha_{m,k}^{n+1}, \alpha_{u,k}^{n+1}\}$ by the obtained optimal solutions and $n = n + 1$.
 - 8: **until** the fractional reduction of the objective function value falls below a predefined threshold $\epsilon_i > 0$.
 - 9: Update $\{\mathbf{W}_k^0, \alpha_{m,k}^0, \alpha_{u,k}^0\}$ by the currently obtained optimal solutions.
 - 10: Update $\eta_1 = \epsilon \eta_1$.
 - 11: **until** the constraint violation falls below a maximum tolerable threshold $\epsilon_o > 0$.
-

following condition:

$$\max \{\|\mathbf{W}_k\|_* - \|\mathbf{W}_k\|_2, \forall k \in \mathcal{K}\} \leq \epsilon_o. \quad (37)$$

The details of the double-layer penalty-based procedure developed for solving problem (27) are summarized in **Algorithm 2**, which is guaranteed to converge to a stationary solution of the original problem (27) [31]. The main computational complexity of **Algorithm 2** arises from iteratively solving problem (27). If the inner-point method of [34] is employed, the complexity of solving problem (27) is on the order of $\mathcal{O}(KN^{3.5} + (6K)^{3.5})$, where $6K$ denotes the number of scalar optimization variables. As a result, the total computational complexity of **Algorithm 2** is given by $\mathcal{O}[I_o^2 I_i^2 (KN^{3.5} + (6K)^{3.5})]$, where I_i^2 and I_o^2 denotes the number of inner and outer iterations required for convergence of **Algorithm 2**.

IV. NUMERICAL RESULTS

In this section, we provide numerical results obtained by Monte Carlo simulations for characterizing the proposed NOMA-aided joint Rad-MU-Com frameworks. In particular, we assume that the DFRC BS employs a uniform linear array (ULA) with half-wavelength spacing between adjacent antennas. The channel between the BS and the R-user is assumed to have pure line-of-sight (LoS) associated with the path loss of $L_R = L_0 + 20\log_{10}d_R$, while between the BS and C-user it is assumed to obey the Rayleigh channel model with the path loss of $L_C = L_0 + 30\log_{10}d_C$ [17,24], where L_0 is the path loss at the reference distance $d = 1$ meter (m), and d_R and d_C represents the distance from the BS to the R-user and to the C-user,

respectively. The parameters adopted in simulations are set as follows: $L_0 = 40$ dB, $d_R = 1000$ m, and $d_C = 100$ m. The noise power in the receiver of users is assumed to be the same, which is set to $\sigma^2 = -100$ dBm. The transmit-signal-to-noise-ratio (SNR)² is considered in the simulations, which is given by $\gamma_p = \frac{P_{\max}}{\sigma^2}$. The initial penalty factors of **Algorithms 1** and **2** are set to $\eta_1 = \eta_2 = 10^4$, the convergence threshold of the inner layer is set to $\epsilon_i = 10^{-2}$, and the algorithm's termination threshold of the equality constraints is set to $\epsilon_o = 10^{-5}$. The numerical results were obtained by averaging over 200 channel realizations.

To obtain the actual true beam pattern, namely \mathbf{R}_0^* of problem (10), the desired beam pattern, $P^*(\theta_m)$, is defined as follows:

$$P^*(\theta_m) = \begin{cases} 1, & \theta_m \in \left[\bar{\theta}_k - \frac{\Delta}{2}, \bar{\theta}_k + \frac{\Delta}{2} \right], \forall k \in \mathcal{K} \\ 0, & \text{otherwise,} \end{cases} \quad (38)$$

where $\{\theta_k, \forall k \in \mathcal{K}\}$ denotes the actual true angles to be detected, which are determined by the location of R-users, and Δ denotes the width of the desired beam, which is set to 10° in the simulation.

A. BB NOMA-Aided Joint Rad-MU-Com System

In the BB NOMA-aided joint Rad-MU-Com system (also referred to as ‘‘BB NOMA+Rad-MU-Com’’), we assume that the R-user is located at the angle of 0° .

1) *Benchmark Schemes*: For performance comparison, we consider the following two benchmark schemes, which have been discussed in **Remark 2**.

- **TDMA-based joint Rad-MU-Com system (also referred to as ‘‘TDMA+Rad-MU-Com’’)**:

In this scheme, the MIMO DFRC BS successively transmits the multicast and unicast messages to the R- and C-users³ over two time slots employing one BF³, which is also used

²Using the transmit-SNR is unconventional, because it is given by the ratio of the transmit power and the receiver noise, which are quantities measured at different points. This quantity is however beneficial for our joint Rad-Com problem, where the optimum transmit power is assigned to each user for satisfying their individual rate requirements under the idealized simplifying assumption that they have perfect capacity-achieving receivers relying on powerful capacity-achieving channel codes. This is because the optimization problem of our specific system was formulated for maximizing the unicast performance at a given transmit power, while satisfying specific constraints imposed both on the multicast rate and on the radar beam pattern.

³In contrast to the communication-only systems, where TDMA can successively employ two different BFs to deliver the multicast and unicast messages, it is practically relevant to assume that the joint Rad-MU-Com system has to employ a common BF for successively conveying different messages, which guarantee that the corresponding beam pattern remains unchanged for radar detection.

for detecting the R-user. Accordingly, for TDMA+Rad-MU-Com, the achievable rate of the multicast signal at the R- and C-users is given by

$$R_{m \rightarrow l}^{\text{TDMA}} = \frac{1}{2} \log_2 \left(1 + \frac{|\mathbf{h}_l^H \mathbf{w}|^2}{\sigma_l^2} \right), \forall l \in \{r, c\}. \quad (39)$$

The corresponding rate of the unicast signal at the C-user is

$$R_u^{\text{TDMA}} = \frac{1}{2} \log_2 \left(1 + \frac{|\mathbf{h}_c^H \mathbf{w}|^2}{\sigma_c^2} \right). \quad (40)$$

The problem of maximizing R_u^{TDMA} can be solved by using **Algorithm 1**, but without the inter-signal interference term.

- **CBF-No-SIC-based joint Rad-MU-Com system (also referred to as “CBF-No-SIC+Rad-MU-Com”)**: In this scheme, the MIMO DFRC BS simultaneously transmits the multicast and unicast messages to the R- and C-users employing two different BFs, which are also jointly used to detect the R-user. All users will directly detect their intended signals by treating others as interference without the assistance of SIC. Therefore, the rate achieved for the unicast signal at the C-user is given by

$$R_u^{\text{CBF-No-SIC}} = \log_2 \left(1 + \frac{|\mathbf{h}_c^H \mathbf{w}_u|^2}{|\mathbf{h}_c^H \mathbf{w}_m|^2 + \sigma_c^2} \right). \quad (41)$$

Note that, for CBF-No-SIC+Rad-MU-Com, the expressions of the rate achieved for the multicast signal at the R- and C-users are the same as (4) and (6). The resultant optimization problem of maximizing $R_u^{\text{CBF-No-SIC}}$ can be solved following a similar process to that of **Algorithm 2** to deal with the interference term in (41).

Although the employment of a single BF in the TDMA+Rad-MU-Com system limits the DoFs compared to that of NOMA and CBF-No-SIC, the advantage is that TDMA supports interference-free transmission for delivering both types of messages. The performance obtained by the proposed NOMA scheme and the two benchmark schemes will be compared in the following.

2) *Unicast Rate Versus $\bar{\gamma}_b$* : In Fig. 5, we investigate the unicast rate, R_u , achieved versus the maximum tolerable beam pattern mismatch, $\bar{\gamma}_b$. We set $\gamma_p = 110$ dB (i.e., $P_{\max} = 10$ dBm) and $\bar{R}_m = 0.5$ bit/s/Hz. As seen in Fig. 5, the unicast rate obtained by all schemes increases as $\bar{\gamma}_b$ increases. This is indeed expected, since larger $\bar{\gamma}_b$ values impose looser constraints on the BF design, which provides higher DoFs, hence enhancing the unicast performance. Moreover,

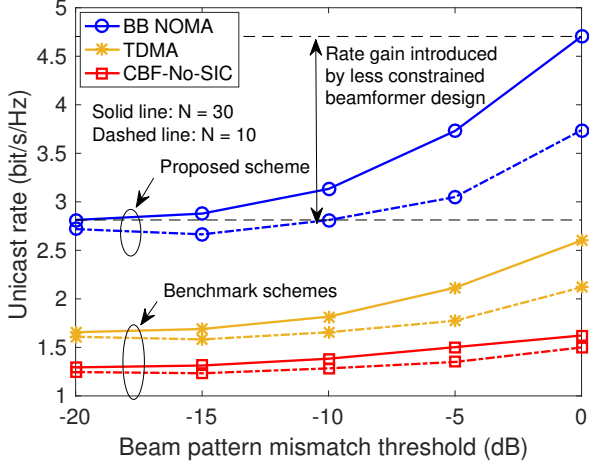


Fig. 5: The unicast rate versus $\bar{\gamma}_b$ for $\gamma_p = 110$ dB and $\bar{R}_m = 0.5$ bit/s/Hz.

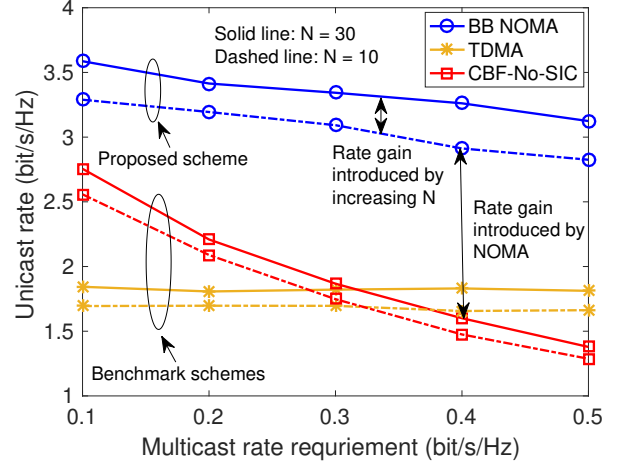


Fig. 6: The unicast rate versus \bar{R}_m for $\gamma_p = 110$ dB and $\bar{\gamma}_b = -10$ dB.

a higher N leads to a higher unicast rate due to the enhanced array gain and spatial DoFs. By comparing the three Rad-MU-Com schemes presented, it may be observed that the proposed BB NOMA+Rad-MU-Com scheme achieves the best performance. This is because on the one hand, employing SIC in NOMA mitigates the inter-signal interference compared to the CBF-No-SIC+Rad-MU-Com scheme, thus improving the unicast performance achieved at the C-user. On the other hand, the power-domain resource sharing and the employment of two different BFs allows NOMA to achieve a higher performance than the TDMA+Rad-MU-Com scheme. Moreover, despite employing a single BF, the TDMA+Rad-MU-Com scheme can deliver both types of messages in an interference-free manner, while carrying out radar detection. Therefore, the TDMA+Rad-MU-Com scheme outperforms the CBF-No-SIC+Rad-MU-Com scheme, whose performance is significantly degraded by the inter-signal interference. It can also be observed that the performance gain obtained by NOMA is more noticeable when $\bar{\gamma}_b$ increases. The above results verify the efficiency of the proposed BB NOMA+Rad-MU-Com framework.

3) *Unicast Rate Versus \bar{R}_m* : In Fig. 6, we investigate the unicast rate, R_u , achieved versus the rate requirement of multicast, \bar{R}_m . We set $\gamma_p = 110$ dB and $\bar{\gamma}_b = -10$ dB. As seen from Fig. 6, NOMA achieves the best performance. Moreover, the unicast rate obtained by NOMA and CBF-No-SIC decreases as \bar{R}_m increases. This is because a higher multicast rate requires more transmit power to be allocated, thus degrading the unicast rate achieved. Without the mitigating assistance of SIC on the inter-signal interference, the degradation of the unicast rate in the CBF-No-SIC+Rad-MU-Com scheme is more significant than that in the proposed BB

NOMA+Rad-MU-Com scheme. Furthermore, the unicast rate obtained by the TDMA+Rad-MU-Com scheme remains almost unchanged. The reason for this trend is as follows. Recall the fact that the TDMA+Rad-MU-Com scheme employs a single common BF for successively delivering the two kinds of messages, where the rate expressions of unicast and multicast at the C-user are the same, see (39) and (40). Therefore, when the rate requirement of multicast is lower than the unicast rate, the impact of \bar{R}_m on the unicast rate becomes negligible, since the multicast rate requirement is automatically satisfied as long as R_u is higher than \bar{R}_m . This also reveals the inefficiency of the fixed resource allocation in TDMA. Additionally, we can observe that the CBF-No-SIC+Rad-MU-Com scheme outperforms the TDMA+Rad-MU-Com scheme when \bar{R}_m is low, but its performance erodes worse when \bar{R}_m increases. This is because, for smaller \bar{R}_m , the unicast transmission of CBF-No-SIC becomes less contaminated by the interference from the multicast signal, thus achieving a higher unicast performance than TDMA due to its full-time transmission. However, when \bar{R}_m becomes stricter, the unicast performance of CBF-No-SIC is significantly degraded by the interference caused by the multicast signal. In this case, the interference-free TDMA outperforms CBF-No-SIC.

4) *Unicast Rate Versus γ_p* : In Fig. 7, we present the unicast rate, R_u , achieved versus the transmit-SNR, γ_p . We set $\bar{R}_m = 0.5$ bit/s/Hz and $\bar{\gamma}_b = -10$ dB. It can be observed that the unicast rate of all schemes increases upon increasing γ_p . However, in contrast to both NOMA and TDMA, the rate enhancement of CBF-No-SIC attained upon increasing γ_p becomes negligible and the unicast rate is seen to be bounded by a certain value. This is because when the inter-signal interference is not mitigated, CBF-No-SIC becomes interference-limited, when the transmit power is high. Moreover, it can also be seen from Fig. 7 that the rate enhancement attained by NOMA upon increasing γ_p is more significant than for TDMA, since NOMA benefits from a flexible resource allocation scheme.

5) *Beam Pattern of a Signal R-User and a Single C-User*: In Fig. 8, we plot the transmit beam pattern obtained by the three schemes for one random channel realization. We set $N = 10$, $\gamma_p = 110$ dB, $\bar{R}_m = 0.5$ bit/s/Hz, and $\bar{\gamma}_b = 0$ dB. In particular, the desired beam pattern is obtained according to (38) and the beam pattern of the radar-only system is obtained by solving problem (10). As illustrated in Fig. 8, the beam pattern obtained by NOMA and TDMA closely approaches that of the radar-only system, while the beam pattern mismatch of CBF-No-SIC becomes more noticeable. Observe in Figs. 5-7 that given the same accuracy requirement of the radar beam pattern, the proposed BB NOMA+Rad-MU-Com scheme achieves higher

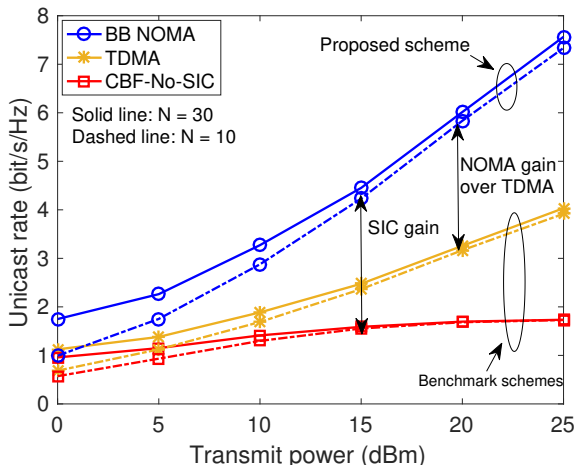


Fig. 7: The unicast rate versus γ_p for $\bar{R}_m = 0.5$ bit/s/Hz and $\bar{\gamma}_b = -10$ dB.

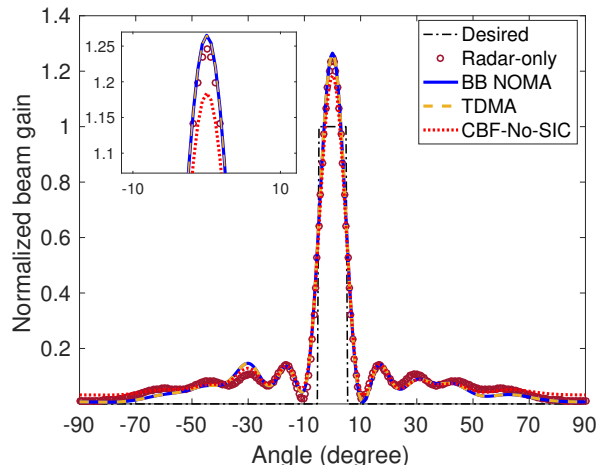


Fig. 8: The transmit beam pattern obtained by different schemes in the considered Rad-MU-Com system with one R-user and one C-user, where $N = 10$, $\gamma_p = 110$ dB, $\bar{R}_m = 0.5$ bit/s/Hz, and $\bar{\gamma}_b = -10$ dB.

communication performance than the other benchmark schemes. The above results also confirm the effectiveness of the proposed BB NOMA+Rad-MU-Com framework.

B. CB NOMA-Aided Joint MIMO Rad-MU-Com System

In the CB NOMA-aided joint Rad-MU-Com system (also referred to as “CB NOMA+Rad-MU-Com”), we consider the case of $K = 3$ R&C pairs, where the 3 R-users are assumed to be located at the angles of $[-60^\circ, 0^\circ, 60^\circ]$. Without loss of generality, the multicast rate requirements of each pair are assumed to be the same, i.e., $\bar{R}_{m,k} = \bar{R}_{m,0}, \forall k \in \mathcal{K}$.

1) *Benchmark Scheme:* We consider the TDMA+Rad-MU-Com as our benchmark scheme⁴. In this case, the DFRC BS successively transmits the unicast and multicast messages employing different BFs intended for each R&C pair. Accordingly, the communication rate attained for the multicast signal of the R- and C-users in the k th pair is given by

$$R_{m \rightarrow l, k}^{\text{TDMA}} = \frac{1}{2} \log_2 \left(1 + \frac{|\mathbf{h}_{l,k}^H \mathbf{w}_k|^2}{\sum_{i \neq k}^K |\mathbf{h}_{l,k}^H \mathbf{w}_i|^2 + \sigma_{l,k}^2} \right), \forall l \in \{r, c\}. \quad (42)$$

⁴As it is impossible for CBF-No-SIC to employ one common BF to deliver two different messages, only the TDMA-based benchmark scheme is considered for the system for multiple R&C pairs.

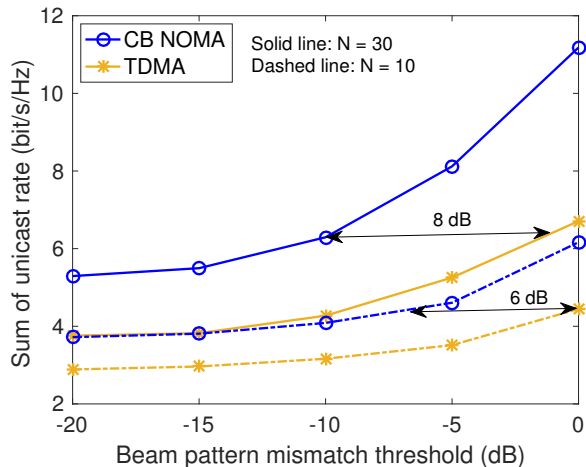


Fig. 9: The sum of the unicast rate versus $\bar{\gamma}_b$ for $\gamma_p = 110$ dB and $\bar{R}_{m,0} = 0.5$ bit/s/Hz.

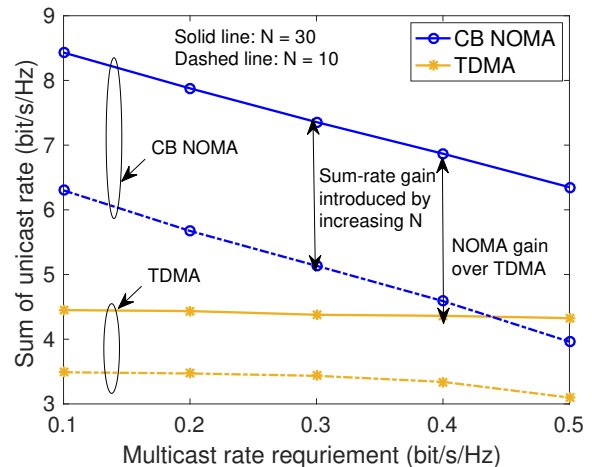


Fig. 10: The sum of the unicast rate versus $\bar{R}_{m,0}$ for $\gamma_p = 110$ dB and $\bar{\gamma}_b = -10$ dB.

Then, the communication rate achieved for the unicast signal at the C-user of the k th pair becomes:

$$R_{u,k}^{\text{TDMA}} = \frac{1}{2} \log_2 \left(1 + \frac{|\mathbf{h}_{c,k}^H \mathbf{w}_k|^2}{\sum_{i \neq k}^K |\mathbf{h}_{c,k}^H \mathbf{w}_i|^2 + \sigma_{c,k}^2} \right). \quad (43)$$

The resultant optimization problem of maximizing $\sum_{k=1}^K R_{u,k}^{\text{TDMA}}$ can be solved by **Algorithm 2**, but without considering the power allocation.

2) *Sum of Unicast Rate Versus $\bar{\gamma}_b$* : In Fig. 9, we investigate the sum of the unicast rate achieved versus the maximum tolerable radar beam pattern mismatch. We set $\gamma_p = 110$ dB and $\bar{R}_{m,0} = 0.5$ bit/s/Hz. Observe that the proposed CB NOMA+Rad-MU-Com scheme outperforms the TDMA+Rad-MU-Com scheme and the sum rate gain of CB NOMA over TDMA becomes more pronounced, when $\bar{\gamma}_b$ increases. A beam pattern mismatch gain of 6 dB and 8 dB can be achieved by CB NOMA over TDMA for $N = 10$ and $N = 30$, respectively. In other words, NOMA can well intergrade both functions of communication and radar detection.

3) *Sum of Unicast Rate Versus $\bar{R}_{m,0}$* : In Fig. 10, we study the sum of the unicast rate versus the multicast rate requirements of each pair. We set $\gamma_p = 110$ dB and $\bar{\gamma}_b = -10$ dB. We can observe that the proposed CB NOMA+Rad-MU-Com scheme outperforms the TDMA+Rad-MU-Com scheme, especially when $\bar{R}_{m,0}$ is small. This reveals that the proposed CB NOMA+Rad-MU-Com scheme is more suitable for scenarios having heterogenous rate requirements. Observe from Fig. 9 that the sum rate gain attained by increasing N for CB NOMA is more significant than

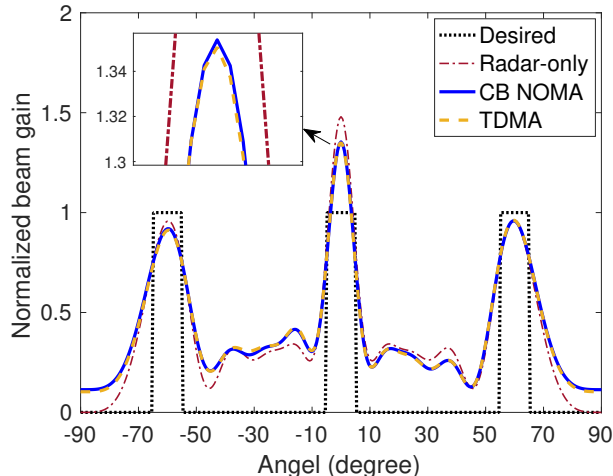


Fig. 11: The transmit beam pattern obtained by different schemes in the joint Rad-MU-Com system with $K = 3$ R&C pairs, where $\gamma_p = 110$ dB, $\bar{R}_{m,0} = 0.5$ bit/s/Hz, and $\bar{\gamma}_b = 0$ dB.

that for TDMA, which means that the proposed CB NOMA+Rad-MU-Com scheme can better exploit the spatial DoFs than TDMA.

4) *Beam Pattern of Multiple R-Users and Multiple C-Users:* In Fig. 11, we present the beam pattern obtained for the Rad-MU-Com system considered having $K = 3$ R&C pairs for a random channel realization. We set $N = 10$, $\gamma_p = 110$ dB, $\bar{R}_{m,0} = 0.5$ bit/s/Hz, and $\bar{\gamma}_b = 0$ dB. Observe that both the beam patterns obtained by CB NOMA and TDMA approach the beam pattern of the radar-only system upon detecting the 3 R-users. However, the communication performance achieved by NOMA is significantly higher than by TDMA, as seen in Figs. 9 and 10. The above results verify that the proposed scheme is eminently suitable for mixed multicast-unicast transmission while well achieving a high-quality beam pattern for multiple target detection in radar.

V. CONCLUSIONS

A novel NOMA-aided joint Rad-MU-Com concept has been proposed, where a MIMO DFRC BS transmits superimposed multicast and unicast messages to the R- and C-users, while detecting the R-user target. The BB NOMA and CB NOMA-aided joint Rad-MU-Com frameworks were proposed for the systems supporting a single and multiple pairs of R- and C-users, respectively. For each framework, tailor-made BF optimization problems were formulated for enhancing the unicast performance, while satisfying both the multicast rate and the radar beam pattern requirements. To solve the resultant non-convex optimization problems, penalty-based iterative

algorithms were developed to find a near-optimal solution. The numerical results obtained revealed that a higher unicast performance can be achieved by the proposed NOMA-aided joint Rad-MU-Com schemes than by the benchmark schemes.

REFERENCES

- [1] Cisco, “Cisco visual networking index: Global mobile data traffic forecast update 2017-2022 white paper,” 2019.
- [2] F. Liu, C. Masouros, A. P. Petropulu, H. Griffiths, and L. Hanzo, “Joint radar and communication design: Applications, state-of-the-art, and the road ahead,” *IEEE Trans. Commun.*, vol. 68, no. 6, pp. 3834–3862, 2020.
- [3] I. S. Merrill, *Introduction to radar systems*. New York, NY, USA: McGraw-Hill, 2001.
- [4] N. C. Luong, X. Lu, D. T. Hoang, D. Niyato, and D. I. Kim, “Radio resource management in joint radar and communication: A comprehensive survey,” *IEEE Commun. Surv. Tut.*, vol. 23, no. 2, pp. 780–814, 2021.
- [5] D. Ma, N. Shlezinger, T. Huang, Y. Liu, and Y. C. Eldar, “Joint radar-communication strategies for autonomous vehicles: Combining two key automotive technologies,” *IEEE Signal Process. Mag.*, vol. 37, no. 4, pp. 85–97, 2020.
- [6] L. Zheng, M. Lops, Y. C. Eldar, and X. Wang, “Radar and communication coexistence: An overview: A review of recent methods,” *IEEE Signal Process. Mag.*, vol. 36, no. 5, pp. 85–99, 2019.
- [7] A. Hassanien, M. G. Amin, E. Aboutanios, and B. Himed, “Dual-function radar communication systems: A solution to the spectrum congestion problem,” *IEEE Signal Process. Mag.*, vol. 36, no. 5, pp. 115–126, 2019.
- [8] R. Saruthirathanaworakun, J. M. Peha, and L. M. Correia, “Opportunistic sharing between rotating radar and cellular,” *IEEE J. Sel. Areas Commun.*, vol. 30, no. 10, pp. 1900–1910, 2012.
- [9] S. Sodagari, A. Khawar, T. C. Clancy, and R. McGwier, “A projection based approach for radar and telecommunication systems coexistence,” in *Proc. IEEE Global Commun. Conf. (GLOBECOM)*, 2012, pp. 5010–5014.
- [10] B. Li, A. P. Petropulu, and W. Trappe, “Optimum co-design for spectrum sharing between matrix completion based MIMO radars and a MIMO communication system,” *IEEE Trans. Signal Process.*, vol. 64, no. 17, pp. 4562–4575, 2016.
- [11] F. Liu, C. Masouros, A. Li, and T. Ratnarajah, “Robust MIMO beamforming for cellular and radar coexistence,” *IEEE Wireless Commun. Lett.*, vol. 6, no. 3, pp. 374–377, 2017.
- [12] J. Qian, M. Lops, L. Zheng, X. Wang, and Z. He, “Joint system design for coexistence of MIMO radar and MIMO communication,” *IEEE Trans. Signal Process.*, vol. 66, no. 13, pp. 3504–3519, 2018.
- [13] F. Liu, C. Masouros, A. Li, T. Ratnarajah, and J. Zhou, “MIMO radar and cellular coexistence: A power-efficient approach enabled by interference exploitation,” *IEEE Trans. Signal Process.*, vol. 66, no. 14, pp. 3681–3695, 2018.
- [14] C. D’Andrea, S. Buzzi, and M. Lops, “Communications and radar coexistence in the massive MIMO regime: Uplink analysis,” *IEEE Trans. Wireless Commun.*, vol. 19, no. 1, pp. 19–33, 2020.
- [15] J. Wang, S. Guan, C. Jiang, D. Alanis, Y. Ren, and L. Hanzo, “Network association in machine-learning aided cognitive radar and communication co-design,” *IEEE J. Sel. Areas Commun.*, vol. 37, no. 10, pp. 2322–2336, 2019.
- [16] A. Hassanien, M. G. Amin, Y. D. Zhang, and F. Ahmad, “Dual-function radar-communications: Information embedding using sidelobe control and waveform diversity,” *IEEE Trans. Signal Process.*, vol. 64, no. 8, pp. 2168–2181, 2016.
- [17] F. Liu, C. Masouros, A. Li, H. Sun, and L. Hanzo, “Mu-MIMO communications with MIMO radar: From co-existence to joint transmission,” *IEEE Trans. Wireless Commun.*, vol. 17, no. 4, pp. 2755–2770, 2018.
- [18] F. Dong, W. Wang, Z. Hu, and T. Hui, “Low-complexity beamformer design for joint radar and communications systems,” *IEEE Commun. Lett.*, vol. 25, no. 1, pp. 259–263, 2021.
- [19] X. Liu, T. Huang, N. Shlezinger, Y. Liu, J. Zhou, and Y. C. Eldar, “Joint transmit beamforming for multiuser MIMO communications and MIMO radar,” *IEEE Trans. Signal Process.*, vol. 68, pp. 3929–3944, 2020.
- [20] F. Liu, L. Zhou, C. Masouros, A. Li, W. Luo, and A. Petropulu, “Toward dual-functional radar-communication systems: Optimal waveform design,” *IEEE Trans. Signal Process.*, vol. 66, no. 16, pp. 4264–4279, 2018.
- [21] X. Wang, A. Hassanien, and M. G. Amin, “Dual-function MIMO radar communications system design via sparse array optimization,” *IEEE Trans. Aerosp. Electron. Syst.*, vol. 55, no. 3, pp. 1213–1226, 2019.
- [22] T. Huang, N. Shlezinger, X. Xu, Y. Liu, and Y. C. Eldar, “MAJoRCom: A dual-function radar communication system using index modulation,” *IEEE Trans. Signal Process.*, vol. 68, pp. 3423–3438, 2020.
- [23] D. Ma, N. Shlezinger, T. Huang, Y. Shavit, M. Namer, Y. Liu, and Y. C. Eldar, “Spatial modulation for joint radar-communications systems: Design, analysis, and hardware prototype,” *IEEE Trans. Veh. Technol.*, vol. 70, no. 3, pp. 2283–2298, 2021.
- [24] N. Su, F. Liu, and C. Masouros, “Secure radar-communication systems with malicious targets: Integrating radar, communications and jamming functionalities,” *IEEE Trans. Wireless Commun.*, vol. 20, no. 1, pp. 83–95, 2021.
- [25] L. Chen, F. Liu, W. Wang, and C. Masouros, “Joint radar-communication transmission: A generalized pareto optimization framework,” *IEEE Trans. Signal Process.*, vol. 69, pp. 2752–2765, 2021.
- [26] Y. Liu, Z. Qin, M. ElKashlan, Z. Ding, A. Nallanathan, and L. Hanzo, “Nonorthogonal multiple access for 5G and beyond,” *Proc. IEEE*, vol. 105, no. 12, pp. 2347–2381, 2017.
- [27] Z. Ding, X. Lei, G. K. Karagiannidis, R. Schober, J. Yuan, and V. K. Bhargava, “A survey on non-orthogonal multiple access for 5G networks: Research challenges and future trends,” *IEEE J. Sel. Areas Commun.*, vol. 35, no. 10, pp. 2181–2195, 2017.

- [28] Y. Liu, H. Xing, C. Pan, A. Nallanathan, M. ElKashlan, and L. Hanzo, "Multiple-antenna-assisted non-orthogonal multiple access," *IEEE Wireless Commun.*, vol. 25, no. 2, pp. 17–23, 2018.
- [29] D. R. Fuhrmann and G. San Antonio, "Transmit beamforming for MIMO radar systems using signal cross-correlation," *IEEE Trans. Aerosp. Electron. Syst.*, vol. 44, no. 1, pp. 171–186, 2008.
- [30] J. Nocedal and S. Wright, *Numerical Optimization*. New York, NY, USA: Springer, 2006.
- [31] Q. T. Dinh and M. Diehl, "Local convergence of sequential convex programming for nonconvex optimization," *Recent Advances in Optimization and its Applications in Engineering*, Springer, 2010.
- [32] M. Grant and S. Boyd, "CVX: Matlab software for disciplined convex programming, version 2.1," [Online]. Available:<http://cvxr.com/cvx>, 2014.
- [33] Z. Luo, W. Ma, A. M. So, Y. Ye, and S. Zhang, "Semidefinite relaxation of quadratic optimization problems," *IEEE Signal Process. Mag.*, vol. 27, no. 3, pp. 20–34, May 2010.
- [34] S. Boyd and L. Vandenberghe, *Convex Optimization*. Cambridge, U.K.: Cambridge Univ. Press, 2004.